Thermodynamic Analysis of Ferrous Ion Binding to *Escherichia coli* Ferritin EcFtnA†

Fadi Bou-Abdallah,*,‡ Mark R. Woodhall,§ Adrián Velázquez-Campoy,|| Simon C. Andrews,§ and N. Dennis Chasteen*,‡

Department of Chemistry, University of New Hampshire, Durham, New Hampshire 03824, Department of Microbiology, School of Animal and Microbial Sciences, University of Reading, Whiteknights, Reading RG6 6AJ, United Kingdom, and Institute of Biocomputation and Complex Systems Physics (BIFI), University of Zaragoza, E-50009 Zaragoza, Spain

Received July 20, 2005; Revised Manuscript Received August 16, 2005

ABSTRACT: Iron oxidation in the bacterial ferritin EcFtnA from *Escherichia coli* shows marked differences from its homologue human H-chain ferritin (HuHF). While the amino acid residues that constitute the dinuclear center in these proteins are highly conserved, EcFtnA has a third iron-binding site (C site) in close proximity to the dinuclear center that is seemingly responsible for these differences. Here, we describe the first thermodynamic study of Fe^{2+} binding to EcFtnA and its variants to determine the location of the primary ferrous ion-binding sites on the protein and to better understand the role of the third C site in iron binding. Isothermal titration calorimetric analyses of the wild-type protein reveal the presence of two main classes of binding sites in the pH range of 6.5−7.5, ascribed to Fe^{2+} binding, first at the A and then the B sites. Site-directed mutagenesis of ligands in the A, B, or C sites affects the apparent Fe^{2+}-binding stoichiometries at the unaltered sites. The data imply some degree of inter- and intrasubunit negative cooperative interaction between sites. Unlike HuHF where only the A site initially binds Fe^{2+}, both A and B sites in EcFtnA bind Fe^{2+}, implying a role for the C site in influencing the binding of Fe^{2+} at the B site of the di-iron center of EcFtnA. The ITC equations describing a binding model for three classes of independent binding sites are reported here for the first time.

Despite its essential role in many metabolic processes, iron can promote oxygen toxicity and generate highly reactive oxygen species (*1*). A variety of efficient mechanisms have been adopted by different organisms to overcome the low solubility and bioavailability of iron, one of which is iron storage by ferritin, a ubiquitous iron biomineralization and detoxification protein (*2*, *3*). Up to 4500 iron atoms can be stored inside the approximately 8 nm cavity of the protein as a mineral iron core that resembles in structure the mineral ferrihydrite, $5Fe_2O_3{\cdot}9H_2O$. In mammals, ferritins consist of 24 subunits of two types, H and L, whereas in microbes and plants, ferritins are homopolymers composed of 24 identical "H-type" subunits. Despite their low amino acid sequence homology (as low as 15% in some cases), typical ferritins from different origins share a conserved three-dimensional structure, where the 24 subunits form a hollow sphere with 4:3:2 symmetry (*1*−*4*). A conserved di-iron ferroxidase center, which is typically embedded within the four-helix bundle of the H but not the L subunits, serves to oxidize Fe^{2+} to Fe^{3+} catalytically.

The bacterium *Escherichia coli* is known to produce at least three different iron-storage proteins that are chemically and structurally different: one bacterioferritin (EcBFR)[1] and two bacterial ferritins (EcFtnA and EcFtnB) (*1*, *5*). Unlike mammalian or bacterial ferritin, bacterioferritin is a heme-containing protein, where up to 12 protoporphyrin IX groups, of unknown function, bind between two subunits with one methionine from each subunit serving as the heme ligand (*1*, *3*−*6*).

Fast oxidation of iron in ferritin is associated with the presence of conserved amino acid residues at the di-iron ferroxidase center of the protein (*1*−*4*). Both EcBFR and EcFtnA rapidly oxidize iron at their ferroxidase centers (*6*−*8*), whereas some of the residues critical for fast iron oxidation are missing in EcFtnB and its function remains unknown (*7*, *9*). EcBFR has the typical di-iron ferroxidase center found in mammalian ferritins, whereas EcFtnA has an additional third iron binding site (C site) that is unique to this protein (*7*, *10*, *11* and Figure 1). Thus, in principle, a total of 72 Fe^{2+} can possibly bind to EcFtnA, one in each of the 24 sites of the A, B, and C trinuclear center. Hydrogen peroxide is the product of dioxygen reduction in the recombinant H-chain ferritin, whereas water is the final product of iron oxidation in EcBFR (*6*, *12*, *13*). In EcFtnA,

† This work was supported by Grant R01 GM20194 from the National Institute of General Medical Sciences (to N.D.C.), the Biotechnology and Biological Sciences Research Council and the University of Reading Research Endowment Trust Fund (to S.C.A.), and by Grant SAF2004-07722 from the Spanish Ministry of Education and Science (A.V.-C.). A.V.-C. is a recipient of a Ramón and Cajal research contract from the Spanish Ministry of Science and Technology.

* To whom correspondence should be addressed. E-mail: fadib@cisunix.unh.edu (F.B.-A.) and ndc@cisunix.unh.edu (N.D.C.). Telephone: 603-862-2520. Fax: 603-862-4278.

‡ University of New Hampshire.

§ University of Reading.

|| University of Zaragoza.

[1] Abbreviations: HuHF, recombinant human H-chain ferritin; MtF, recombinant human mitochondrial ferritin; EcBFR, *E. coli* bacterioferritin; EcFtnA and EcFtnB, *E. coli* bacterial ferritins types A and B, respectively; ITC, isothermal titration calorimetry; Mes, 2-(*N*-morpholino)ethanesulfonic acid; Mops, 3-(*N*-morpholino)propanesulfonic acid; His53A, A-site variant of EcFtnA; E94A, B-site variant of EcFtnA; E126A and E49A, C-site variants of EcFtnA; E130A, B- and C-site variant of EcFtnA.

10.1021/bi0514212 CCC: $30.25 © 2005 American Chemical Society
Published on Web 09/30/2005

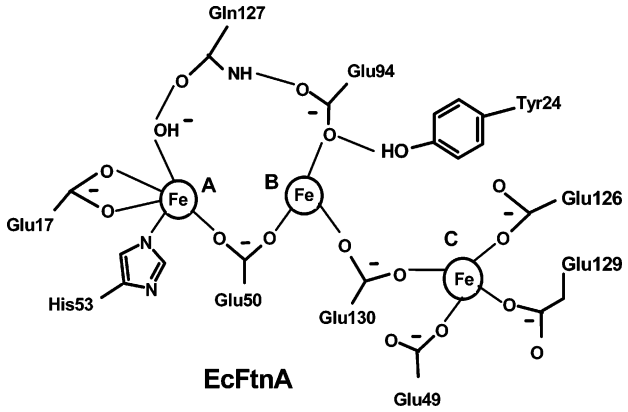

FIGURE 1: Diagram showing the dinuclear ferroxidase center (A and B) and the third proximal C site of EcFtnA from *E. coli*. The drawing is based on the crystal structure of the Fe^{3+} derivative of EcFtnA (*11*) and was made with the ISIS Draw 2.4 program manufactured by MDL (Molecular Design Limited, www.mdl.com).

an odd iron oxidation stoichiometry of ~3.5 Fe^{2+}/O_2 is observed, suggesting that hydrogen peroxide is a byproduct of oxygen reduction in this protein (*7*).

Isothermal titration calorimetry (ITC) has been shown to be an excellent tool for studying metal ion binding to amino acids, peptides, and proteins in solution (*14*−*19*). In a recent investigation, we used ITC to determine the number and location of the primary binding sites for Fe^{2+} in recombinant H-chain ferritin and their affinity for iron (*14*). In addition, we have identified with the aid of site-directed mutagenesis the principal pathway by which Fe^{2+} travels to the dinuclear ferroxidase center of the H-subunit prior to its oxidation to Fe^{3+} (*14*, *15*). To our knowledge, there have been no direct studies of Fe^{2+} binding to EcFtnA, and the primary binding sites for Fe^{2+} on this protein remain unknown. The identity of these sites in EcFtnA is particularly important because of the presence of the third iron-binding site (C site) in close proximity to the di-iron ferroxidase center. Comparatively little is known about the effect of this site on the iron-binding and oxidation properties of the protein.

Here, we again use ITC to elucidate the primary Fe^{2+}-binding sites in the recombinant bacterial ferritin (EcFtnA) and to define the thermodynamic profile of this interaction. The results of this study show that, under anaerobic conditions and dilute protein solutions (3−5 μM) at pH 6.5−7.5, at least two classes of Fe^{2+}-binding sites are observed in the wild-type (WT) protein. The first class of strong binding sites corresponds to binding of ~24 Fe^{2+}/protein at pH 7.0 to the histidine containing site A at the ferroxidase center, similarly to what has been previously observed with HuHF (*14*). Mutation of the ferroxidase center residue (H53A) at the A site eliminates the first class of strong Fe^{2+}-binding sites, confirming the involvement of the histidine-containing A site in the initial and strong Fe^{2+} binding. The second class of binding sites is pH-independent and corresponds to binding of an additional 24 Fe^{2+}/protein to the B site of the dinuclear center in the pH range of 6.5−7.5. Consistent with the X-ray data, Zn^{2+} titration into the apoprotein showed the presence of mainly two classes of binding sites each with a stoichiometry of ~24 Zn^{2+}/protein, ascribed to Zn^{2+} binding to the dinuclear sites A and B (*10*). Complicated binding isotherms with multiple classes of binding sites quite different from those observed for the WT protein were obtained for various site-directed mutants of the A-, B-, and C-site ligands, indicating a strong interdependence among the sites in their ability to complex iron. The binding equations for three classes of independent binding sites are reported here for the first time and used to fit the complex isotherms encountered in this study (see the Materials and Methods).

MATERIALS AND METHODS

All chemicals were of reagent grade and used directly without further purification: ferrous sulfate heptahydrate, $FeSO_4 \cdot 7H_2O$ (J. T. Baker Chemical Co.), zinc sulfate heptahydrate, $ZnSO_4 \cdot 7H_2O$ (Mallinckrodt Chemical Works), Mes and Mops (Research Organics, Inc.), and 2,2′-dipyridyl and sodium chloride (Aldrich Chemical Co.).

Site-directed mutagenesis was performed on the *E. coli* ferritin A (EcFtnA) gene (*ftnA*) carried by the plasmid pGS761 (pAlterEx1 plus *ftnA*, Ap^R; *8*) using a modified QuickChange method (Stratagene) in which the antibiotic resistance genes were not targeted and electrocompenent *E. coli* XL1-Blue (Stratagene) was used for transformations. All site-directed variants were produced using pairs of mutagenic PCR primers to introduce the desired codon changes. The identity of each site-directed mutant was confirmed by determining the nucleotide sequence (MWG AG Biotech, U.K.) of the entire *ftnA* structural gene. EcFtnA and its variants were overexpressed and purified as described previously (*20*) except that MRW2 [BL21/λDE3-Star *ftnA*; F^-, *ompT*, *hsdS*$_B$, (r_B^-, m_B^-), *dcm*, *gal*, *rne131*, Δ*ftnA*::*spc*, λDE3] was the host strain and 1 mM IPTG was added to induce expression once the optical density (at 650 nm) of cultures reached 0.5. Any residual iron was subsequently removed from the pure proteins by dialysis against sodium hydrosulfite (dithionite), $Na_2S_2O_4$, and 2,2′-bipyridyl at pH 6.0 (*21*). Protein concentrations were determined spectrophotometrically using the molar absorptivity of 24 000 cm^{-1} M^{-1} at 280 nm for the apoprotein (this paper).

ITC measurements were carried out at 25.00 °C on an upgraded CSC Model 4200 isothermal titration calorimeter (Calorimetry Science Corporation). The fundamental principles of ITC are described elsewhere (*22*). All of the experiments were conducted under anaerobic conditions using 1 mM dithionite ($Na_2S_2O_4$) and an atmosphere of argon to prevent Fe^{2+} oxidation from possible residual O_2. Each ITC titration was carried out using a 250 μL syringe and consecutive injections of 10 μL titrant into the ITC reaction cell containing the protein solution with stirring at 297 rpm (*14*). To correct for dilution and mixing effects, a series of control injections was carried out, in which small aliquots of ferrous or zinc sulfate solutions prepared in the same buffer as the protein were titrated into buffer alone. The heat signal of the control was then subtracted from the raw data obtained for ferritin. In variant H53A, where only two classes of binding sites are observed, the ITC analysis software from CSC was used to fit the data and the values of the fitting parameters were then confirmed with our developed model of three sets of independent binding sites in which n_1, K_1, and ΔH_1 were set equal to 0. The errors given in Table 1 from curve fitting are from replicate measurements. Conditions for the individual experiments are given in the figure captions.

ITC Data Analysis. A model of three classes of independent binding sites was employed to analyze the calorimetric titrations. The macromolecule, M, contains three sets of

independent binding sites for the ligand, L, with binding affinities K_j, binding enthalpies ΔH_j, and stoichiometries n_j ($j = 1$, 2, and 3). To fit the experimental data, it is necessary to estimate the heat associated with any injection in the calorimeter. To do that, the concentration of all species in equilibrium, free and bound, after each injection i, must be calculated from the total concentration of the macromolecule $[M]_T$ and ligand $[L]_T$ in the calorimetric cell. Briefly, from the mass balance equations for the macromolecule and the ligand and the chemical equilibrium equations (mass action law, where it is assumed that activity coefficients are equal to unity), it is possible to express the total concentration of ligand $[L]_T$ in terms of the concentration of free ligand [L], the total concentration of the macromolecule, and the binding affinity and stoichiometry of each class of binding sites (*23*, *24*)

$$[L]_T = [L] + [M]_T\left(\frac{n_1K_1[L]}{1+K_1[L]} + \frac{n_2K_2[L]}{1+K_2[L]} + \frac{n_3K_3[L]}{1+K_3[L]}\right) \quad (1)$$

where the second term on the right side is the concentration of ligand bound to the macromolecule, $[L]_B$, and each of the terms inside the parenthesis is the number of ligand molecules bound per macromolecule for each class of sites, $[L]_{B,j}/[M]_T$, where $[L]_{B,j}$ is the concentration of ligand bound to the class j of binding sites. It is possible to rearrange eq 1 to arrive at a quartic polynomial equation in terms of a more convenient variable, the free ligand molar fraction, $x \equiv [L]/[L]_T$

$$ax^4 + bx^3 + cx^2 + dx + e = 0 \quad (2)$$

where the parameters a, b, c, d, and e are given by

$$a = \beta_3$$

$$b = \frac{1}{[L]_T}(\beta_2 + \alpha_3[M]_T - \beta_3[L]_T)$$

$$c = \frac{1}{[L]_T^2}(\beta_1 + \alpha_2[M]_T - \beta_2[L]_T)$$

$$d = \frac{1}{[L]_T^3}(1 + \alpha_1[M]_T - \beta_1[L]_T)$$

$$e = -\frac{1}{[L]_T^3} \quad (3)$$

and the α's and β's are given by

$$\alpha_1 = n_1K_1 + n_2K_2 + n_3K_3$$

$$\alpha_2 = (n_1+n_2)K_1K_2 + (n_1+n_3)K_1K_3 + (n_2+n_3)K_2K_3$$

$$\alpha_3 = (n_1+n_2+n_3)K_1K_2K_3$$

$$\beta_1 = K_1 + K_2 + K_3$$

$$\beta_2 = K_1K_2 + K_1K_3 + K_2K_3$$

$$\beta_3 = K_1K_2K_3 \quad (4)$$

Solving eq 2 allows the calculation of the concentration of free ligand and, therefore, the concentration of ligand bound to the class j of binding sites

$$[L]_{B,j} = [M]_T\frac{n_jK_j[L]}{1+n_jK_j[L]} \quad (5)$$

Although an exact analytical solution is possible for other less complex binding equilibrium systems (*22*), in our case, which involves a quartic algebraic equation, a numerical solution is more convenient. To solve eq 2 numerically for any set of assumed values for n_j and K_j, the Newton−Raphson method was employed. This iterative algorithm is easy to implement and is characterized by a very fast convergence (*25*). If $f(x) = 0$ is the equation to be solved, a sequence of values x_k is generated starting with an initial value x_0

$$x_{k+1} = x_k - \frac{f(x_k)}{f'(x_k)} \quad (6)$$

where $f'(x)$ is the derivative of the function $f(x)$, until the convergence criterion is satisfied

$$|x_{k+1} - x_k| < \epsilon \quad (7)$$

Values of 0.5 and 10^{-15} for x_0 and ϵ, respectively, were used, and convergence was achieved before 10 iterations in every case.

After each injection i, the total concentrations of the macromolecule and ligand in the calorimetric cell are given by

$$[M]_{T,i} = [M]_0\left(1 - \frac{v}{V}\right)^i$$

$$[L]_{T,i} = [L]_0\left(1 - \left(1 - \frac{v}{V}\right)^i\right) \quad (8)$$

where $[M]_0$ is the initial concentration of macromolecule in the cell, $[L]_0$ is the concentration of ligand in the syringe, v is the injection volume, and V is the cell volume.

As stated above, solving eq 2 for each injection i in the calorimeter allows the estimation of the composition of the solution in the calorimetric cell after any injection, and therefore, it is possible to calculate the heat associated with any injection i, q_i

$$q_i = Q_i - Q_{i-1}\left(1 - \frac{v}{V}\right) = V\sum_{j=1}^{3}\left(\Delta H_j\left([L]_{B,j,i} - [L]_{B,j,i-1}\left(1 - \frac{v}{V}\right)\right)\right) + q_d \quad (9)$$

where $[L]_{B,j,i}$ is the concentration of ligand bound to the class j of binding sites after injection i. The term q_d is introduced to account for a residual heat effect after complete saturation of the macromolecule and reflects nonspecific injection and dilution phenomena. Thermodynamic binding parameters (K_j, ΔH_j, and n_j) were estimated through nonlinear least-squares fitting of the experimental data using eq 9, employing the Levenberg−Marquardt minimization algorithm.

RESULTS

Fe^{2+} Binding to WT EcFtnA. The heats produced from the anaerobic incremental additions of Fe^{2+} to the wild-type

Table 1: Best Fit Parameters for ITC Measurements of Fe^{2+} and Zn^{2+} Binding to EcFtnA and Its Variants at 25.00 °C[a]

protein	n_1	K_1 (M^{-1})	$\Delta H_1°$ (kJ/mol)	$\Delta S_1°$[b] [J/(mol K)]	$\Delta G_1°$[c] (kJ/mol)	n_2	K_2 (M^{-1})	$\Delta H_2°$ (kJ/mol)	$\Delta S_2°$[b] [J/(mol K)]	$\Delta G_2°$[c] (kJ/mol)	$n_3K_3\Delta H_3°$
WT EcFtnA and Fe^{2+} at pH 7.0	21.1 ± 0.5	(3.5 ± 0.8) × 10^6	3.4 ± 0.2	136.5 ± 2.1	−37.3 ± 0.6	19.8 ± 0.7	1.8 ± 0.4) × 10^5	9.9 ± 0.3	133.8 ± 2.2	−30.0 ± 0.6	(8.5 ± 16.1) × 10^5
WT EcFtnA and Fe^{2+} at pH 6.50	11.2 ± 0.2	(3.5 ± 0.3) × 10^5	11.7 ± 0.2	145.2 ± 1.0	−31.6 ± 0.2	19.5 ± 0.3	(4.6 ± 0.3) × 10^4	25.5 ± 0.5	174.8 ± 1.8	−26.6 ± 0.2	(4.2 ± 3.8) × 10^5
His53A, A-site variant and Fe^{2+} at pH 7.0						26.5 ± 3.9	(3.4 ± 0.4) × 10^3	29.1 ± 5.6	165.3 ± 18.8	−20.2 ± 0.3	very weak
E94A, B-site variant and Fe^{2+} at pH 7.0	7.1 ± 0.1	(1.7 ± 0.3) × 10^7	−4.9 ± 0.2	122.1 ± 1.5	−41.3 ± 0.4	13.5 ±0.1	(1.3 ± 0.1) × 10^6	−9.5 ± 0.1	85.2 ± 0.7	−34.9 ± 0.2	(1.8 ± 0.3) × 10^6
E126A, C-site variant and Fe^{2+} at pH 7.0	6.7 ± 0.2	(2.2 ± 0.5) × 10^7	5.3 ± 0.2	158.3 ± 2.1	−41.9 ± 0.6	31.6 ± 0.2	(3.5 ± 0.5) × 10^6	2.2 ± 0.1	132.5 ± 1.4	−37.3 ± 0.4	(2.7 ± 1.9) × 10^6
E49A, C-site variant and Fe^{2+} at pH 7.0	10.3 ± 2.1	(2.1 ± 0.3) × 10^7	4.4 ± 1.0	155.0 ± 3.5	−41.8 ± 0.3	42.2 ± 3.5	(2.2± 0.2) × 10^6	−1.1 ± 0.2	117.7 ± 1.0	−36.2 ± 0.2	(7.8 ± 3.1) × 10^6
E130A, B- and C-site variant and Fe^{2+} at pH 7.0	7.8 ± 0.2	(5.4 ± 5.4) × 10^7	10.4 ± 0.1	182.8 ± 8.4	−44.1 ± 2.5	16.1 ±0.2	(3.2 ± 0.5) × 10^5	9.1 ± 0.1	135.8 ± 1.4	−31.4 ± 0.4	(7.2 ± 0.8) × 10^6
WT EcFtnA and Zn^{2+} at pH 7.0	4.2 ± 1.2	(1.0 ± 0.1) × 10^7	1.2 ± 0.7	138.2 ± 2.5	−40.0 ± 0.2	22.1 ±0.5	(3.7 ± 0.2) × 10^6	−24.4 ± 0.2	44.0 ± 0.7	−37.5 ± 0.1	$n_3 = 27.7 \pm 0.8$ $K_3 = (9.6 \pm 0.8) \times 10^3\ M^{-1}$ $\Delta H_3° = 47.9 \pm 1.3$ kJ/mol $\Delta S_3° = 236.9 \pm 1.6$ J/(mol K) $\Delta G_3° = -22.7 \pm 0.2$ kJ/mol

[a] The reported thermodynamic parameters are apparent values including contributions to the overall equilibrium from ferritin and buffer species in different states of protonation. Standard errors from replicate determinations are indicated. The errors associated with each class of sites were obtained from fits where the parameters of the other two classes of sites were fixed. [b] Calculated from $\Delta S° = (\Delta H° - \Delta G°)/T$. [c] Calculated from $\Delta G° = -RT \ln K$.

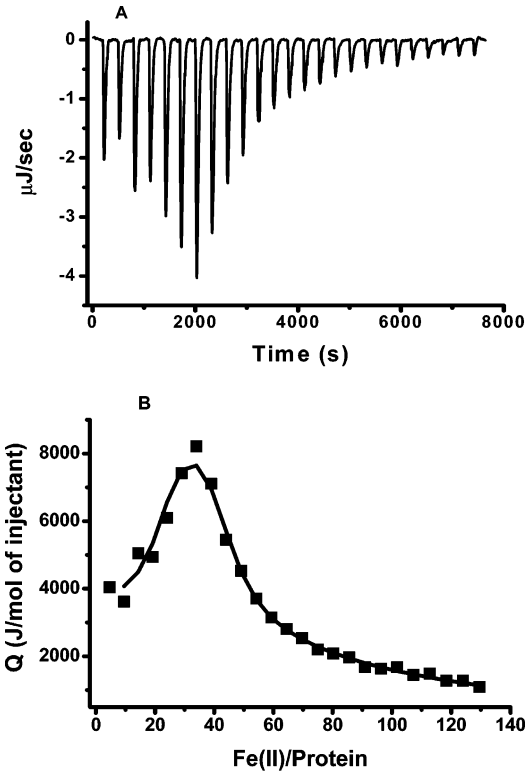

FIGURE 2: Calorimetric titration of WT EcFtnA with Fe^{2+} under anaerobic conditions. (A) Raw data. (B) Plot of the integrated heat versus the Fe^{2+}/protein molar ratio. Conditions: 4.725 μM EcFtnA titrated with 10 μL injections of 3.12 mM $FeSO_4$. Both protein and Fe^{2+} solutions are in 100 mM Mops buffer, 50 mM NaCl, and 1 mM $Na_2S_2O_4$ at pH 7.0 and 25.00 °C.

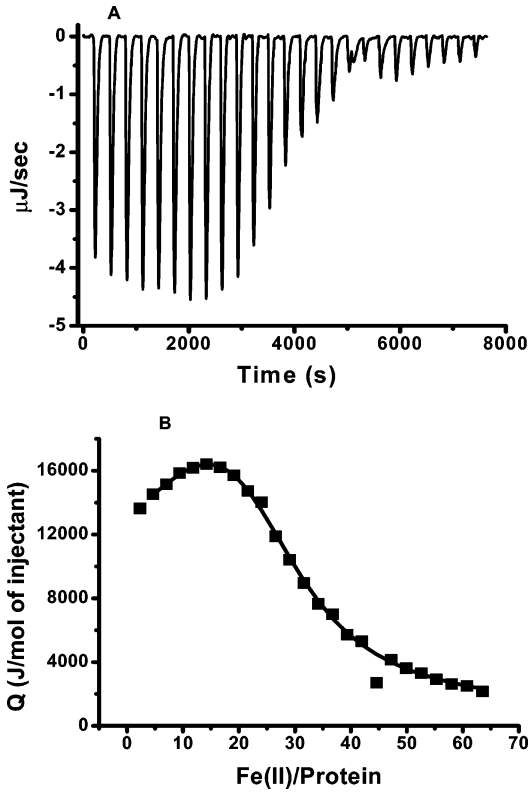

FIGURE 3: Calorimetric titration of WT EcFtnA with Fe^{2+} under anaerobic conditions. (A) Raw data. (B) Plot of the integrated heat versus the Fe^{2+}/protein molar ratio. Conditions: 5.5 μM EcFtnA titrated with 10 μL injections of 1.78 mM $FeSO_4$. Both protein and Fe^{2+} solutions are in 100 mM Mes buffer, 50 mM NaCl, and 1 mM $Na_2S_2O_4$ at pH 6.50 and 25.00 °C.

EcFtnA at pH 7.0 are shown in Figure 2A. The integrated heats (μJ) for each injection as a function of the molar ratio of Fe^{2+} to the apoprotein are displayed in Figure 2B. As shown in Figure 2A, Fe^{2+} titration into an anaerobic EcFtnA solution produces two strong endothermic reactions (negative peaks correspond to an endothermic reaction in the CSC isothermal titration calorimeter). The heats at the end of the titration in Figure 2 are in excess of the heats of dilution from Fe^{2+} in buffer alone, indicating the presence of additional weak iron binding to the protein. Accordingly, a model of three sets of independent binding sites was used to curve fit the data (see the Materials and Methods), where an excellent fit is achieved (Figure 2B). (The data could not be fitted with the CSC BindWorks software, which handles only two classes of independent binding sites.) The resulting parameters are summarized in Table 1.

The first two classes of independent binding sites, one strong and the other weak, are well-resolved with stoichiometries of $n_1 \sim 21$ and $n_2 \sim 20$ Fe^{2+}/protein for each class of sites at pH 7.0 (Figure 2). At a lower pH of 6.5, the anaerobic titration of WT EcFtnA with Fe^{2+} resulted in a binding isotherm with a first inflection point at $n_1 \sim 11$ Fe^{2+}/EcFtnA for the first class of strong binding sites and a second inflection point at $n_2 \sim 20$ Fe^{2+}/EcFtnA for the second class of weaker binding sites (Figure 3). These results indicate that the first class of strong binding sites most likely involves binding of Fe^{2+} at the A sites that contain a histidine residue, because histidine pK_a values are typically in this pH range. A recent ITC investigation of Fe^{2+} binding to HuHF has shown that His65 at the A site of this protein is responsible for the first strong class of binding sites (*14*), similarly to EcFtnA. The second class of weaker sites ($n_2 \sim 20$) could involve binding at either the B or C site of the protein, but zinc/iron competitive binding data presented below combined with published X-ray data indicate that binding occurs at the B site (*11*, *29*).

The individual thermodynamic parameters of the third class of very weak binding sites cannot be determined under the dilute solution conditions of the ITC experiment (Table 1), and only the product $n_3K_3\Delta H_3$ is obtained (Table 1). These very weak binding sites may reflect nonspecific binding to the protein or weak binding to functional sites.

Fe^{2+} Binding to A-Site Variant H53A. To gain more insight into the location of Fe^{2+}-binding sites on the protein, several variants of EcFtnA were prepared. H53A is an A-site variant, where the coordinating ligand, His53, is mutated to the noncoordinating ligand, alanine. The effect of this mutation on the iron-binding stoichiometry resulted in the elimination of the first class of strong Fe^{2+}-binding sites (Figure 4), thereby confirming the identity of the 24 A sites as primary Fe^{2+}-binding sites on the protein. Only the second class of binding sites (n_2) with additional weak binding at the third class of sites (n_3) is observed. Accordingly, a model consisting of two sets of independent binding sites, one strong (n_2) and the other weak (n_3), was used to curve fit the data in Figure 4, and the derived parameters are summarized in Table 1. Similarly to the WT EcFtnA, variant H53A displays an endothermic reaction for Fe^{2+} binding with a binding stoichiometry of $n_2 \sim 26$ Fe^{2+}/protein but with a binding affinity of approximately 360 times weaker than that of the n_2 sites of the WT protein (Table 1). Thus, the mutation of

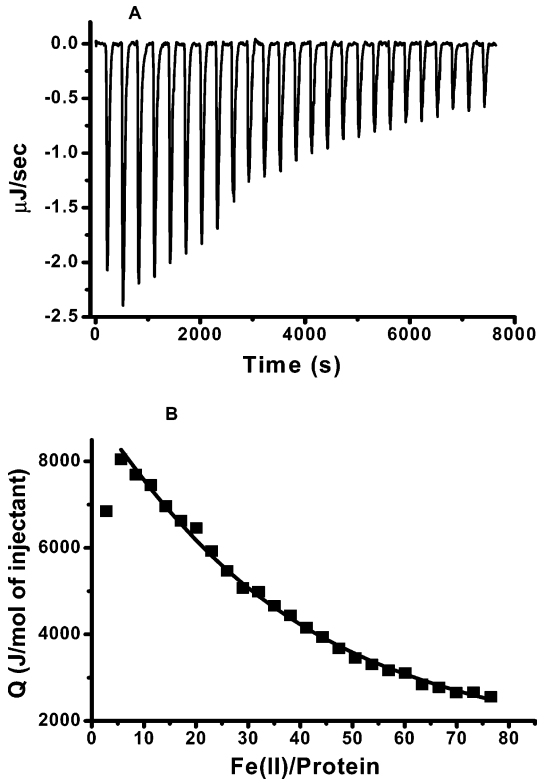

FIGURE 4: Calorimetric titration of A-site variant (His53A) of EcFtnA with Fe^{2+} under anaerobic conditions. (A) Raw data. (B) Plot of the integrated heat versus the Fe^{2+}/protein molar ratio. Conditions: 5.0 μM His53A titrated with 10 μL injections of 1.95 mM $FeSO_4$. Both protein and Fe^{2+} solutions are in 100 mM Mops buffer, 50 mM NaCl, and 1 mM $Na_2S_2O_4$ at pH 7.0 and 25.00 °C.

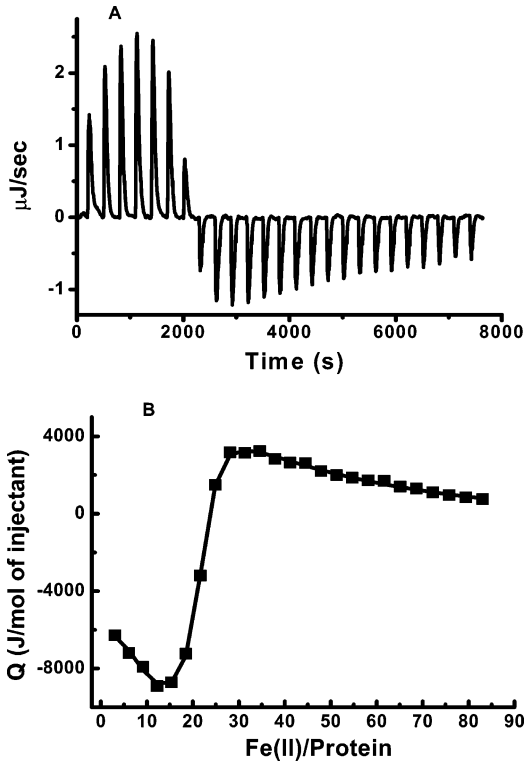

FIGURE 5: Calorimetric titration of B-site variant (E94A) of EcFtnA with Fe^{2+} under anaerobic conditions. (A) Raw data. (B) Plot of the integrated heat versus the Fe^{2+}/protein molar ratio. Conditions: 5.0 μM EcFtnA titrated with 10 μL injections of 1.95 mM $FeSO_4$. Both protein and Fe^{2+} solutions are in 100 mM Mops buffer, 50 mM NaCl, and 1 mM $Na_2S_2O_4$ at pH 7.0 and 25.00 °C.

the His53 ligand of the A site causes a loss in A-site binding but also weakens the strength of Fe^{2+} binding at the B site.

Fe^{2+} Binding to B-Site Variant E94A. In contrast to variant H53A and to the WT protein, variant E94A, a B-site variant, displays exothermic heats for the first two classes of sites (n_1 and n_2) and an endothermic heat for the third class of weak sites (n_3) when the apoprotein is titrated with Fe^{2+} in Mops buffer at pH 7.0 (Figure 5). Accordingly, the Fe^{2+}-binding isotherm was fitted to a model consisting of three classes of independent binding sites (Figure 5B and Table 1). Apparent binding stoichiometries of $n_1 \sim 7$ and $n_2 \sim 13$ Fe^{2+}/protein were obtained. It is clear that the mutation of residue E94 of the B site has a profound effect on both the n_1 and n_2 binding stoichiometries. This result does not unequivocally establish the location of the Fe^{2+}-binding sites in this variant, but as discussed below, these apparent stoichiometries most likely represent binding at either the A and/or B sites. The values of n_3, K_3, and ΔH_3 for the third class of binding sites cannot be measured independently, but their product was determined to be $(1.8 \pm 0.3) \times 10^6$ (Table 1).

Fe^{2+} Binding to C-Site Variants E126A and E49A. Fe^{2+} titration into the C-site variant E126A shows at least three endothermic binding events in Mops buffer at pH 7.0. Despite the complex pattern of this isotherm as shown in Figure 6B, a very good fit was obtained using a model of three sets of independent binding sites (Table 1). Here again, apparent Fe^{2+}-binding stoichiometries of $n_1 \sim 7$ and $n_2 \sim 32$ Fe^{2+}/protein are obtained with this variant. However, because the maximum binding stoichiometry of any of the three sites A, B, or C is ~24 Fe^{2+}/site, these apparent stoichiometries (i.e., $n_1 + n_2 = 39$ Fe^{2+}/protein) probably represent the total Fe^{2+}-binding stoichiometry of both A and B sites (more below). In the C-site variant E49A, a similar pattern for Fe^{2+} titration is observed (Figure 7) with somewhat higher Fe^{2+}-binding stoichiometries (i.e., $n_1 \sim 10$ and $n_2 \sim 42$ Fe^{2+}/protein) than variant E126A (Table 1). The product of the three thermodynamic parameters ($n_3K_3\Delta H_3$) for the weakest sites are reported in Table 1.

Fe^{2+} Binding to B- and C-Site Variant E130A. Glu130 is a bridging ligand between the B and C site with average metal−ligand distances of 2.38 and 1.89 Å, respectively, for the two sites of the Fe^{3+} derivative (*11*). When Fe^{2+} is titrated anaerobically into the apoprotein solution of E130A, two binding isotherms with endothermic heats of reaction are observed (Figure 8). The first isotherm corresponds to a first class of sites with an apparent binding stoichiometry of $n_1 \sim 8$ Fe^{2+}/protein and high binding affinity ($\sim 5 \times 10^7$ M^{-1}) similar to the B- and C-site variants, E94A and E126A, respectively (Table 1). As to the second class of sites, an apparent binding stoichiometry of $n_2 \sim 16$ Fe^{2+}/protein is observed similar to the B-site variant E94. However, the Fe^{2+}-binding affinity is weakened from $\sim 1 \times 10^6$ M^{-1} in variant E94A to $\sim 3 \times 10^5$ M^{-1} in variant E130A (Table 1).

Zn^{2+} Binding to WT EcFtnA. To gain further knowledge about the strong binding sites of Fe^{2+} on the protein, we examined the thermodynamics of Zn^{2+} binding to the apoprotein. Zn^{2+}, among other metal ions, has been often used to probe Fe^{2+} binding and oxidation in ferritins (*10*, *15*, *26*) and has been recently used in the crystal structure determination of EcFtnA, where it is found bound at both

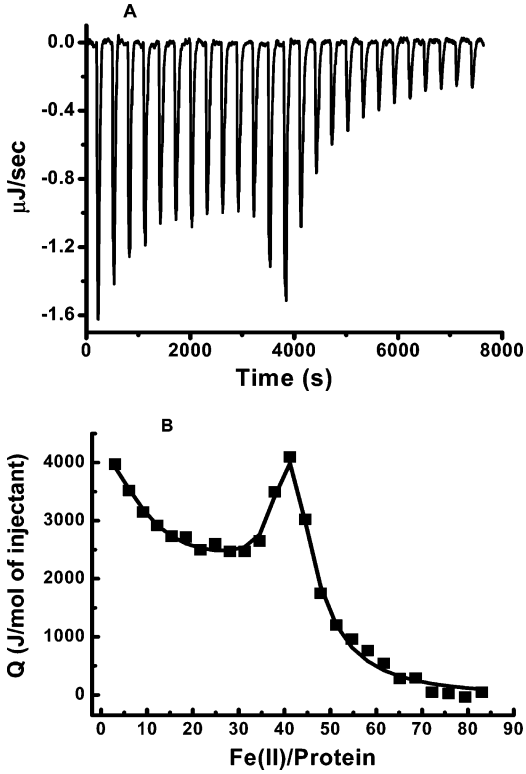

FIGURE 6: Calorimetric titration of C-site variant (E126A) of EcFtnA with Fe^{2+} under anaerobic conditions. (A) Raw data. (B) Plot of the integrated heat versus the Fe^{2+}/protein molar ratio. Conditions: 5.0 μM EcFtnA titrated with 10 μL injections of 1.95 mM $FeSO_4$. Both protein and Fe^{2+} solutions are in 100 mM Mops buffer, 50 mM NaCl, and 1 mM $Na_2S_2O_4$ at pH 7.0 and 25.00 °C.

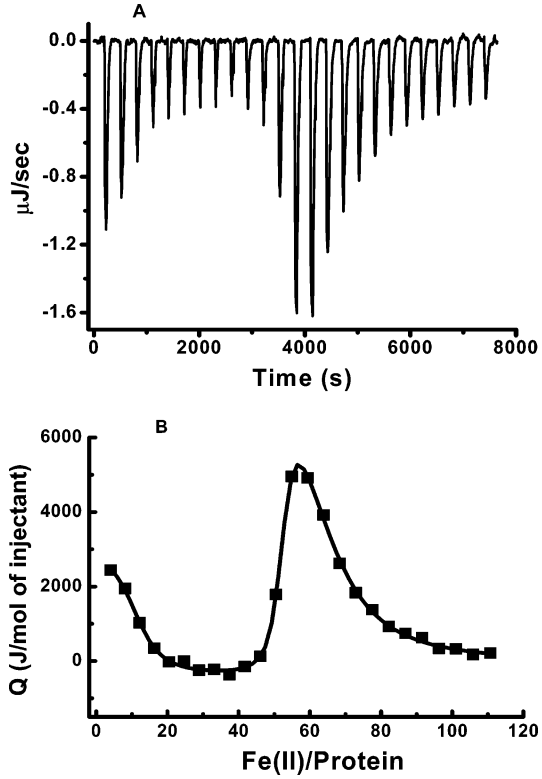

FIGURE 7: Calorimetric titration of C-site variant (E49A) of EcFtnA with Fe^{2+} under anaerobic conditions. (A) Raw data. (B) Plot of the integrated heat versus the Fe^{2+}/protein molar ratio. Conditions: 3.75 μM EcFtnA titrated with 10 μL injections of 1.95 mM $FeSO_4$. Both protein and Fe^{2+} solutions are in 100 mM Mops buffer, 50 mM NaCl, and 1 mM $Na_2S_2O_4$ at pH 7.0 and 25.00 °C.

the A and B sites (*11*, 29). Figure 9 shows the raw ITC data and the integrated heats from zinc binding to WT EcFtnA in Mops buffer at pH 7.0. The data suggest the presence of three classes of binding sites and were therefore fitted using a model with three sets of independent binding sites. Interestingly, the derived parameters for the first two classes of sites show similar binding affinities for Zn and a total binding stoichiometry ($n_1 + n_2$) of ~26 molar equivalents/protein (Table 1). The third class of sites has a much lower affinity for Zn^{2+} (Table 1) but a binding stoichiometry of $n_3 \sim 28$ Zn^{2+}/protein.

Because the X-ray structure of the Zn^{2+} derivative of EcFtnA shows saturation of the A and B site with Zn^{2+}, we assume that the first and second classes ($n_1 + n_2 \sim 26$) of binding sites observed here by ITC represent Zn^{2+} binding to the A site, while the third class of sites ($n_3 \sim 28$) represents Zn^{2+} binding to the B site. To confirm this assertion, an ITC competition experiment between Fe^{2+} and Zn^{2+} was performed at pH 7.0, in which 48 Zn^{2+} were first added to the apoprotein under anaerobic conditions followed by titration with Fe^{2+}. No Fe^{2+} binding isotherm was observed (data not shown) when the protein was preloaded with a stoichiometric amount of Zn^{2+} (i.e., 2 Zn^{2+}/subunit), a result confirming the binding of Zn^{2+} at the dinuclear sites A and B and its competition with Fe^{2+}. Under the conditions of this experiment (3.2 μM protein, 48 Zn^{2+}/protein, and 4 Fe^{2+}/injection/protein in 0.1 M Mops and 50 mM NaCl at pH 7.0), constant and very small heats of reaction were observed that were in slight excess of the heat of dilution and possibly correspond to the very weak association of Fe^{2+} with the protein (i.e., a third class of binding sites) as discussed above for Fe^{2+}. When Zn^{2+} or Fe^{2+} were titrated into the apoprotein at pH 7.5, higher binding affinities but similar apparent stoichiometries to those reported at pH 7.0 were obtained.[2] Therefore, the negative cooperativity between binding sites in EcFtnA appears to be pH-dependent and is associated with high binding affinities (i.e., $K \geq 10^7$ M^{-1}) of the two metal ions to the initial class of A sites (Table 1).

DISCUSSION

In the present study, we have characterized the thermodynamic interaction of Fe^{2+} with WT EcFtnA and its site-directed variants. The advantage of ITC is that all thermodynamic parameters (i.e., binding stoichiometry *n*, binding affinity *K*, enthalpy $\Delta H°$, entropy $\Delta S°$, and Gibbs free energy $\Delta G°$) can be determined in a single experiment. However, when complex binding isotherms with multiple overlapping binding events are involved, the analysis of the data can become a challenge. The present study demonstrates for the first time that such complex isotherms can be successfully

[2] Thermodynamic parameters of Zn^{2+} titration into EcFtnA at pH 7.5 ($n_1 = 3.7 \pm 0.4$, $K_1 = (1.4 \pm 0.1) \times 10^8$ M^{-1}, $\Delta H_1 = 2.4 \pm 1.0$ kJ/mol, $n_2 = 21.6 \pm 0.4$, $K_2 = (3.2 \pm 0.2) \times 10^7$ M^{-1}, $\Delta H_2 = -31.6 \pm 0.2$ kJ/mol, $n_3 = 21.2 \pm 0.3$, $K_3 = (6.8 \pm 0.3) \times 10^4$ M^{-1}, $\Delta H_3 = 33.9 \pm 0.1$ kJ/mol). Thermodynamic parameters of Fe^{2+} titration into EcFtnA at pH 7.5 ($n_1 = 3.1 \pm 0.4$, $K_1 = (3.3 \pm 1.8) \times 10^7$ M^{-1}, $\Delta H_1 = 7.9 \pm 1.0$ kJ/mol, $n_2 = 18.5 \pm 0.4$, $K_2 = (9.3 \pm 3.8) \times 10^6$ M^{-1}, $\Delta H_2 = 3.2 \pm 0.2$ kJ/mol, $n_3 = 15.1 \pm 2.8$, $K_3 = (1.9 \pm 0.5) \times 10^4$ M^{-1}, $\Delta H_3 = 18.0 \pm 4.2$ kJ/mol). Thus, similarly to all B and C variants, the first few metal ions that bind to the WT protein (i.e., $n_1 \sim 3-4$, at pH 7.0−7.50 for Zn^{2+} and at pH 7.50 for Fe^{2+}) negatively affect the binding of subsequent metal ions at the same sites on the protein.

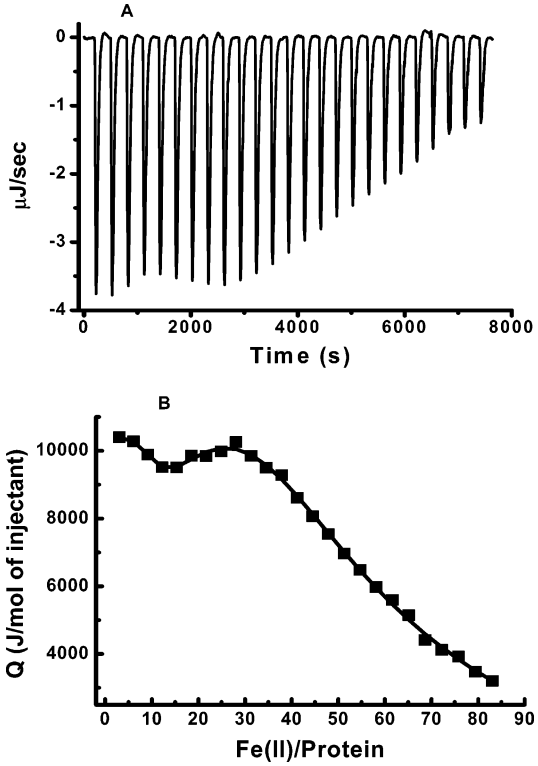

FIGURE 8: Calorimetric titration of B- and C-site variant (E130A) of EcFtnA with Fe^{2+} under anaerobic conditions. (A) Raw data. (B) Plot of the integrated heat versus the Fe^{2+}/protein molar ratio. Conditions: 5.0 μM EcFtnA titrated with 10 μL injections of 1.95 mM $FeSO_4$. Both protein and Fe^{2+} solutions are in 100 mM Mops buffer, 50 mM NaCl, and 1 mM $Na_2S_2O_4$ at pH 7.0 and 25.00 °C.

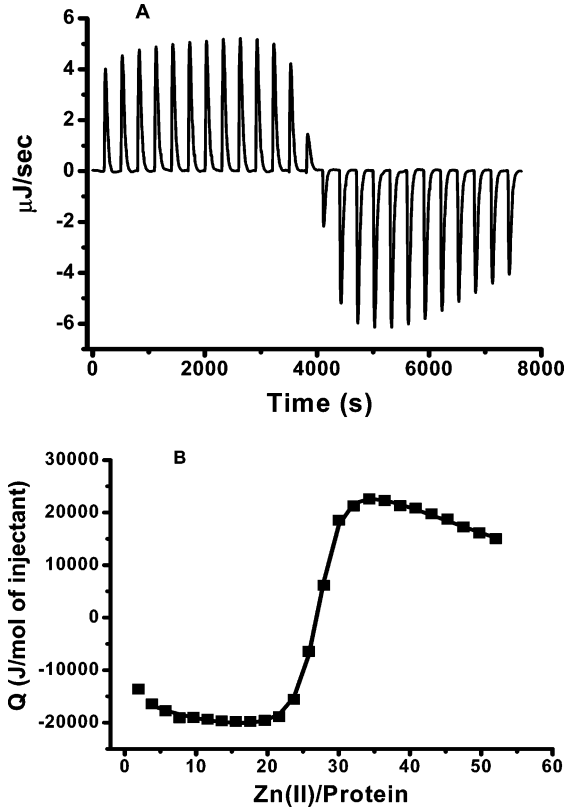

FIGURE 9: Calorimetric titration of WT EcFtnA with Zn^{2+}. (A) Raw data. (B) Plot of the integrated heat versus the Fe^{2+}/protein molar ratio. Conditions: 6.65 μM EcFtnA titrated with 10 μL injections of 1.625 mM $ZnSO_4$. Both protein and Zn^{2+} solutions are in 100 mM Mops buffer and 50 mM NaCl at pH 7.0 and 25.00 °C.

simulated and that previously noninterpretable isotherms (*30*) may yield to a similar analysis. However, the binding model employed here assumes independent binding sites, which is rigorously not the case as seen with the site-directed variants, where mutation of one ligand in any of the three sites (A, B, or C) affects binding at the other two sites and the n_1 and n_2 stoichiometries are either greater or less than the theoretical value of 24 metal ions/class of sites (Table 1). These effects suggest some degree of intra- and intersubunit cooperativity in binding as discussed below. Despite these effects and the markedly different binding isotherms (Figures 2−9), excellent curve fits are obtained using a model of multiple independent binding sites with good agreement between the apparent thermodynamic parameters from replicate determinations. Finally, the fact that all of the mutations perturb the binding stoichiometries strongly argues that binding principally occurs at the ferroxidase center of the protein.

Our ITC results indicate that at pH 7.0 the first class of sites ($n_1 \sim 24$) corresponds to Fe^{2+} binding at the A sites followed by a second class of sites ($n_2 \sim 24$) assigned to Fe^{2+} binding at the B sites (Figure 2 and Table 1). These findings are in accordance with stopped-flow and ITC investigations of Fe^{2+} binding and oxidation in EcFtnA and HuHF, where a preferred order of Fe^{2+} binding to site A and then to site B was observed followed by fast oxidation of the diferrous complex (*14*, *27*). While the A-site variant H53A conclusively demonstrates that the first class of sites are those involving A sites (see the Results), there are four principal lines of evidence supporting the assignment of the second class of sites to the B sites. First, the apparent binding stoichiometries of ($n_1 + n_2$) ~ 39 and 50 in the C-site variants (E126A and E49A) are consistent with simultaneous binding of Fe^{2+} to both A and B sites corresponding to almost full saturation of the dinuclear centers. In accordance with this interpretation, Mössbauer and X-ray studies have shown the presence of iron at the A and B sites but not at the C site of variant E49A (*10*, *29*). Second, the apparent binding stoichiometries for the second class of sites are lowest for the B-site variants E94A and E130A, an observation consistent with partial occupancy of these sites and the importance of residues E94 and E130 in Fe^{2+} binding at the B site (Table 1). Third, previous Zn^{2+} and Tb^{3+} competition experiments showed that iron oxidation occurs at the A and B sites of variant E130A with very little iron at the C site, a result consistent with our ITC data and with A and B sites being the primary sites of Fe^{2+} binding and oxidation (*10*). Fourth, the X-ray structure of WT EcFtnA showed similar structural positions of the A- and B-site residues in the Fe^{3+}-free and Fe^{3+}-bound structures, indicating very little or no residue reorientation of the Fe^{3+}-binding structure (*11*). In contrast, the Zn^{2+}-binding structure showed more movement of side chains at the di-iron center. The X-ray data are consistent with our ITC observations (Figures 2, 3, and 9 and Table 1), where the Fe^{2+}-binding isotherms in the WT protein consisted of mainly two classes of binding sites at the di-iron center A and B, whereas the Zn^{2+} titration shows three classes of sites that possibly reflect the flexibility of the side-chain ligands in Zn^{2+} binding.

Alteration of any of the A-, B-, or C-site ligands in EcFtnA (i.e., His53, Glu94, Glu130, Glu126, or Glu49) results in

pronounced changes in the overall Fe^{2+}-binding properties of the protein, a result indicating that all of these residues are important in Fe^{2+} binding and that all three sites are highly interactive (Table 1). All variants, except His53A, show the presence of at least three classes of binding sites in which the first $n_1 \sim 7-10$ Fe^{2+} ions that bind to the protein appear to influence the binding of subsequent Fe^{2+} ($n_2 \sim 13-42$) such that the total ($n_1 + n_2$) Fe^{2+} stoichiometry is ~24 for saturation of A sites or ~48 for saturation of A and B sites. This type of behavior can be rationalized if we assume that there is some degree of negative cooperativity between ferroxidase centers in the binding of Fe^{2+}, whereby the binding of the first few Fe^{2+} ions to the protein decreases the affinity of subsequently bound Fe^{2+} to varying degrees depending upon the variant under study (Table 1). Consistent with this scheme, a recent study of iron binding and oxidation in the mitochondrial ferritin MtF suggested the presence of negative cooperativity between the ferroxidase centers, whereby only half of the 24 ferroxidase centers of MtF bind and oxidize Fe^{2+} (*28*).

One of the important questions in the bacterial ferritin EcFtnA is the role of the third C site. Previous studies have suggested a role for this site in influencing the iron oxidation stoichiometry and the fate of the oxidized iron. In addition, it has been shown that the presence of the C site is not essential for fast oxidation of Fe^{2+} at the dinuclear centers but rather increases the iron turnover rate of these centers (*7*). Our ITC data indicate that the C site is not a strong Fe^{2+}-binding site but that its presence influences the binding of Fe^{2+} at the dinuclear ferroxidase center. Thus, while HuHF binds only 1 Fe^{2+}/subunit at the A site initially (*14*), EcFtnA binds 2 Fe^{2+}/subunit, one at each of the dinuclear sites A and B.

In the case of Zn^{2+} binding to WT EcFtnA, the ITC data reveal an initial endothermic reaction followed by exothermic and then endothermic events (Table 1). The first few Zn^{2+} to bind ($n_1 \sim 4$) have high binding affinity followed by additional Zn^{2+} binding to the same sites but with slightly weaker affinity until saturation is achieved at ($n_1 + n_2$) ~ 26, which is essentially the theoretical stoichiometry of 24 Zn^{2+}/site (Figure 9 and Table 1). The third binding event exhibits endothermic heats of reaction with lower affinity but a binding stoichiometry of ~ 28 Zn^{2+}/protein corresponding to saturation of all B sites (~1 Zn^{2+}/site). This interpretation is in agreement with the X-ray crystallographic data of the Zn^{2+} derivative of EcFtnA, showing full occupancy of the A and B sites of the protein by Zn^{2+} (*11*, *29*) with no Zn^{2+} found at the C site. This is also consistent with Zn^{2+} being an inhibitor of iron oxidation in EcFTnA presumably because Zn^{2+} competes with Fe^{2+} ions for the dinuclear ferroxidase sites (*10*, *26*). The Zn^{2+}/Fe^{2+} ITC competition experiment further supports this assignment (see the Results) and indicates that Zn^{2+} and Fe^{2+} compete for the same binding sites on the protein.

The large positive entropy values [average $\Delta S^\circ \sim 140$ J/(mol K)] obtained with all protein samples (Table 1) indicate that Fe^{2+} binding to EcFtnA is entropically driven as previously observed with Fe^{2+}, Zn^{2+}, and Tb^{3+} binding to HuHF and other proteins (*14*, *15*, *18*, *19*). The B-site variant E94A is the only variant to exhibit both favorable enthalpy and entropy changes (Table 1). Under similar experimental conditions and in the pH range of 6.5−7.5, the Fe^{2+}- and Zn^{2+}-binding affinities for EcFtnA are similar to those for HuHF within the experimental errors (*14*, *15* and Table 1).

In summary, despite the complex binding isotherms, the present work has identified the primary Fe^{2+}-binding sites in EcFtnA and helped to clarify the molecular events prior to iron oxidation. The ITC results confirm previous observations that suggested that the A sites are the preferred and strongest Fe^{2+}-binding sites on the protein. In the WT EcFtnA and at pH 7.0, two main classes of binding sites were observed corresponding to binding of ~24 Fe^{2+} at each of the two sites of the di-iron ferroxidase center. At a higher pH of 7.0−7.5, there appears to be a degree of negative cooperativity between binding sites, whereby the first few Fe^{2+} or Zn^{2+} ions to bind at the A sites lower the affinity of metal ions for the other ferroxidase centers. The third binding site in EcFtnA (C site) does not appear to be involved in strong Fe^{2+} binding, at least initially, but seems to modulate Fe^{2+} binding at the adjacent dinuclear iron sites A and B.

REFERENCES

1. Andrews, S. C. (1998) Iron storage in bacteria, *Adv. Microb. Physiol. 40*, 281−351.
2. Chasteen, N. D., and Harrison, P. M. (1999) Mineralization in ferritin: An efficient means of iron storage, *J. Struct. Biol. 126*, 182−194.
3. Chasteen, N. D. (1998) Ferritin. Uptake, storage, and release of iron, in *Metal Ions in Biological Systems* (Sigel, H., and Sigel, A., Eds.) Vol. 35, pp 479−514, Marcel Dekker, Inc., New York.
4. Harrison, P. M., and Arosio, P. (1996) The ferritins: Molecular properties, iron storage function, and cellular regulation, *Biochim. Biophys. Acta 1275*, 161−203.
5. Smith, J. L. (2004) The physiological role of ferritin-like compounds in bacteria, *Crit. Rev. Microbiol. 30*, 173−185.
6. Yang, X., Le Brun, N. E., Thomson, A. J., Moore, G. R., and Chasteen, N. D. (2000) The iron oxidation and hydrolysis chemistry of *Escherichia coli* bacterioferritin, *Biochemistry 39*, 4915−4923.
7. Treffry, A., Zhao, Z., Quail, M. A., Guest, J. R., and Harrison, P. M. (1998) How the presence of three iron binding sites affects the iron storage function of the ferritin (EcFtnA) of *Escherichia coli*, *FEBS Lett. 432*, 213−218.
8. Treffry, A., Zhao, Z., Quail, M. A., Guest, J. R., and Harrison, P. M. (1995) Iron(II) oxidation by H-chain ferritin: Evidence from site-directed mutagenesis that a transient blue species is formed at the dinuclear iron center, *Biochemistry 34*, 15204−15213.
9. Harrison, P. M., Hempstead, P. D., Artymiuk, P. J., and Andrews, S. C. (1998) Structure−function relationships in the ferritins, in *Metal Ions in Biological Systems* (Sigel, H., and Sigel, A., Eds.) Vol. 35, pp 435−477, New York.
10. Bauminger, E. R., Treffry, A., Quail, M. A., Zhao, Z., Nowik, I., and Harrison, P. M. (2000) Metal binding at the active centre of the ferritin of *Escherichia coli* (EcFtnA). A Mössbauer spectroscopic study, *Inorg. Chim. Acta 297*, 171−180.
11. Stillman, T. J., Hempstead, P. D., Artymiuk, P. J., Andrews, S. C., Hudson, A. J., Treffry, A., Guest, J. R., and Harrison, P. M. (2001) The high-resolution X-ray crystallographic structure of the ferritin (EcFtnA) of *Escherichia coli*; comparison with human H ferritin (HuHF) and the structures of the Fe^{3+} and Zn^{2+} derivatives, *J. Mol. Biol. 307*, 587−603.
12. Bou-Abdallah, F., Lewin, A. C., Le Brun, N. E., Moore, G. R., and Chasteen, N. D. (2002) Iron detoxification properties of *Escherichia coli* bacterioferritin. Attenuation of oxyradical chemistry, *J. Biol. Chem. 277*, 37064−37069.
13. Zhao, G., Bou-Abdallah, F., Yang, X., Arosio, P., and Chasteen, N. D. (2001) Is hydrogen peroxide produced during iron(II) oxidation in mammalian apoferritins? *Biochemistry 40*, 10832−10838.
14. Bou-Abdallah, F., Arosio, P., Santambrogio, P., Yang, X., Janus-Chandler, C., and Chasteen, N. D. (2002) Ferrous ion binding to recombinant human H-chain ferritin. An isothermal titration calorimetry study, *Biochemistry 41*, 11184−11191.

15. Bou-Abdallah, F., Arosio, P., Levi, S., Janus-Chandler, C., and Chasteen, N. D. (2003) Defining metal ion inhibitor interactions with recombinant human H- and L-chain ferritins and site-directed variants: An isothermal titration calorimetry study, *J. Biol. Inorg. Chem. 8*, 489−497.
16. Zhang, Y., Akilesh, S., and Wilcox, D. E. (2000) Isothermal titration calorimetry measurements of Ni^{II} and Cu^{II} binding to His, GlyGlyHis, HisGlyHis, and bovine serum albumin: A critical evaluation, *Inorg. Chem. 39*, 3057−3064.
17. Zhang, Y., and Wilcox, D. E. (2002) Thermodynamic and spectroscopic study of Cu^{II} and Ni^{II} binding to bovine serum albumin, *J. Biol. Inorg. Chem. 7*, 327−337.
18. Bou-Abdallah, F., Adinolfi, S., Pastore, A., Laue, T. M., and Chasteen, N. D. (2004) Iron binding and oxidation kinetics in frataxin CyaY of *Escherichia coli*, *J. Mol. Biol. 341*, 605−615.
19. Su, M., Cavallo, S., Stefanini, S., Chiancone, E., and Chasteen, N. D. (2005) The so-called listeria innocua ferritin is a Dps protein. Iron incorporation, detoxification, and DNA protection properties, *Biochemistry 44*, 5572−5578.
20. Hudson, A. J., Andrews, S. C., Hawkins, C., Williams, J. M., Izuhara, M., Meldrum, F. C., Mann, S., Harrison, P. M., and Guest, J. R. (1993) Overproduction, purification, and characterization of the *Escherichia coli* ferritin, *Eur. J. Biochem. 218*, 985−995.
21. Bauminger, E. R., Harrison, P. M., Hechel, D., Nowik, I., and Treffry, A. (1991) Mössbauer spectroscopic investigation of structure−function relations in ferritins, *Biochim. Biophys. Acta 1118*, 48−58.
22. Freire, E., Mayorga, O. L., and Straume, M. (1990) Isothermal titration calorimetry, *Anal. Chem. 62*, 950A−959A.
23. Wyman, J., and Gill, S. J. (1990) *Binding and Linkage: Functional Chemistry of Biological Macromolecules*, University Science Books, Mill Valley, CA, chapters 2 and 3.
24. Cantor, C. R., and Schimmel, P. R. (1980) *Biophysical Chemistry. Part III: The Behavior of Biological Macromolecules*, W. H. Freeman and Co, New York, chapter 15.
25. Press, W. H., Flannery, B. P., Teukolsky, S. A., and Vetterling, W. T. (1992) *Numerical Recipes in C: The Art of Scientific Computing*, Cambridge University Press, New York, pp 362−368.
26. Treffry, A., Zhao, Z., Quail, M. A., Guest, J. R., and Harrison, P. M. (1998) The use of zinc(II) to probe iron binding and oxidation by the ferritin (EcFtnA) of *Escherichia coli*, *J. Biol. Inorg. Chem. 3*, 682−688.
27. Treffry, A., Zhao, Z., Quail, M. A., Guest, J. R., and Harrison, P. M. (1997) Dinuclear center of ferritin: Studies of iron binding and oxidation show differences in the two iron sites, *Biochemistry 36*, 432−441.
28. Bou-Abdallah, F., Santambrogio, P., Levi, S., Arosio, P., and Chasteen, N. D. (2005) Unique iron binding and oxidation properties of human mitochondrial ferritin: A comparative analysis with human H-chain ferritin, *J. Mol. Biol. 347*, 543−554.
29. Stillman, T. J., Connolly, P. P., Latimer, C. L., Morland, A. F., Quail, M. A., Andrews, S. C., Treffry, A., Guest, J. R., Artymiuk, P. J., and Harrison, P. M. (2003) Insights into the effects on metal binding of the systematic substitution of five key glutamate ligands in the ferritin of *Escherichia coli*, *J. Biol. Chem. 278*, 26275−26286.
30. Chao, Y., and Fu, D. (2004) Thermodynamic studies of the mechanism of metal binding to the *Escherichia coli* zinc transporter YiiP, *J. Biol. Chem. 279*, 17173−17180.

BI0514212